

Out-of-Equilibrium Kondo Effect: Response to Pulsed Fields

Avraham Schiller¹ and Selman Hershfield²

¹ *Racah Institute of Physics, The Hebrew University, Jerusalem 91904, Israel*

² *Department of Physics and National High Magnetic Field Laboratory, University of Florida, PO Box 118440, Gainesville, FL 32611*

(October 31, 2018)

The current in response to a rectangular pulsed bias potential is calculated exactly for a special point in the parameter space of the nonequilibrium Kondo model. Our simple analytical solution shows the all essential features predicted by the non-crossing approximation, including a hierarchy of time scales for the rise, saturation, and fall-off of the current; current oscillations with a frequency of eV/\hbar ; and the instantaneous reversal of the fall-off current for certain pulse lengths. Rich interference patterns are found for a nonzero magnetic field (either dc or pulsed), with several underlying time scales. These features should be observable in ultra small quantum dots.

PACS numbers: 72.15.Qm, 72.10.Fk, 73.50.Mx

The recent observation of the Kondo effect in ultra small quantum dots¹⁻⁴ has focused considerable attention on the Kondo effect in mesoscopic systems. Acting as tunable Anderson impurities, quantum-dot devices offer an outstanding opportunity to test some of the basic notions of the Anderson impurity model.⁵ For example, the crossover from the local-moment to the mixed-valent and empty-impurity regimes,¹ the $\pi/2$ phase shift associated with the Kondo effect,⁶ and the evolution of the Kondo effect with dc⁷⁻⁹ and ac¹⁰⁻¹² bias potentials. Most recently, an intriguing scenario for the response of a quantum dot to a rectangular pulsed bias potential was put forward by Plihal *et al.*¹³ Using a time-dependent version of the non-crossing approximation, these authors predicted a hierarchy of time scales for the rise, saturation, and fall-off of the current through the dot, featuring a rich interplay between the Kondo temperature, the applied voltage bias, and the temperature. For larger values of the pulsed bias eV , oscillations were predicted in the time-dependent current, with a characteristic frequency of $\omega = eV/\hbar$. These current oscillations were attributed to the sharp excitation frequency between the two split Kondo peaks induced by the eV bias potential.¹⁴

In this paper, we exploit an exactly solvable nonequilibrium Kondo model^{9,11} to obtain a simple analytic description of the Kondo-assisted current in response to rectangular pulsed fields. Our solution captures all the essential features reported by Plihal *et al.*,¹³ including the hierarchy of time scales for the rise, saturation, and fall-off of the current; the eV/\hbar oscillations in the time-dependent current; and the instantaneous reversal of the current – for certain pulse lengths – after the pulse has ended. Furthermore, we are able to include also a nonzero magnetic field which itself can be pulsed, revealing complex interference patterns between the bias and magnetic field. Most importantly, since our solution is analytic and exact, it provides a benchmark result for the response of a quantum dot to pulsed fields.

We begin with a few general remarks on the solvable

model used. An extension of the Toulouse¹⁵ and Emery-Kivelson¹⁶ solutions of the equilibrium Kondo problem to nonequilibrium,¹⁷ this model is expected to correctly describe the strong-coupling regime of the nonequilibrium Kondo effect. Indeed, previous applications of the model to dc⁹ and ac¹¹ bias potentials have shown all the qualitative features of Kondo-assisted tunneling: A zero-bias anomaly that splits in an applied magnetic field; Fermi-liquid characteristics in the low- T and low- V differential conductance; Side peaks in the differential conductance at $eV = \pm n\hbar\omega$, for an ac drive of frequency ω . At the same time, since the solvable point involves strong couplings, this model is incapable of describing weak-coupling features such as the logarithmic temperature dependence of the conductance at elevated T .

Introducing the actual physical system, it consists of two noninteracting leads of spin-1/2 electrons, interacting via a spin-exchange coupling with a spin-1/2 impurity moment $\vec{\tau}$ placed in between the two leads. The impurity moment can represent either an actual magnetic impurity or a quantum dot with a single unpaired electron. Each lead is subject to a separate time-dependent potential, such that a time-dependent voltage bias forms across the junction. Since the interaction with the impurity is local in space (s -wave scattering), one can reduce the conduction-electron degrees of freedom that couple to the impurity to one-dimensional fields $\psi_{\alpha\sigma}(x)$, where $\alpha = R, L$ labels the lead (right or left) and $\sigma = \uparrow, \downarrow$ specifies the spin orientations. In terms of these one-dimensional fields, coupling to the impurity takes place via the local spin densities $\vec{s}_{\alpha\beta} = \frac{1}{2} \sum_{\sigma, \sigma'} \psi_{\alpha\sigma}^\dagger(0) \vec{\sigma}_{\sigma, \sigma'} \psi_{\beta\sigma'}(0)$.

As discussed in detail in Refs. 9 and 11, the exactly solvable model corresponds to a particular choice of the spin-exchange couplings, described by the Hamiltonian

$$\mathcal{H} = \mathcal{H}_0 - \sum_{\alpha=L,R} eV_\alpha(t) \hat{N}_\alpha - \mu_B g_i H(t) \tau^z + \sum_{\alpha, \beta=L,R} J_\perp^{\alpha\beta} \left\{ s_{\alpha\beta}^x \tau^x + s_{\alpha\beta}^y \tau^y \right\}, \quad (1)$$

$$\mathcal{H}_0 = i\hbar v_F \sum_{\alpha=L,R} \sum_{\sigma=\uparrow,\downarrow} \int_{-\infty}^{\infty} \psi_{\alpha\sigma}^\dagger(x) \frac{\partial}{\partial x} \psi_{\alpha\sigma}(x) dx + J_z (s_{LL}^z + s_{RR}^z) \tau^z. \quad (2)$$

Here the inter-lead longitudinal couplings have been set equal to zero, while the intra-lead longitudinal couplings take the value $J_z = 2\pi\hbar v_F$. The three transverse couplings J_\perp^{LL} , J_\perp^{RR} , and $J_\perp^{LR} = J_\perp^{RL}$ are arbitrary. \hat{N}_α and $V_\alpha(t)$ in the second term of Eq. (1) are the number operator and time-dependent potential on lead α , respectively, while $H(t)$ is a local magnetic field acting on the impurity spin.

The basic approach we take is identical to that of Ref. 11, where the same system was solved for ac drives. The first step is to convert the interacting nonequilibrium problem to a noninteracting one. To this end, we first decompose the Hamiltonian into an unperturbed part and a perturbation, where the unperturbed part consists of \mathcal{H}_0 and the time-dependent voltage $V_\alpha(t)$. The initial density matrix — characterizing the distribution of the unperturbed system before tunneling has been switched on — is equal to $\rho_0 = e^{-\beta\mathcal{H}_0}/\text{Trace}\{e^{-\beta\mathcal{H}_0}\}$.

The Hamiltonian, its unperturbed part, and the initial density matrix are then converted to quadratic forms via the following sequence of steps:^{9,16} (i) Bosonizing the fermion fields; (ii) Converting to new boson fields corresponding to collective charge (c), spin (s), flavor (f), and spin-flavor (sf) excitations; (iii) Performing a canonical transformation; (iv) Refermionizing the new boson fields by introducing four new fermion fields, $\psi_\mu(x)$ with $\mu = c, s, f, sf$; and (v) Representing the impurity spin (which has been mixed by the canonical transformation with the conduction-electron spin degrees of freedom) in terms of two Majorana fermions: $\hat{a} = -\sqrt{2}\tau_y$ and $\hat{b} = -\sqrt{2}\tau_x$. For $J_z = 2\pi\hbar v_F$, one thus arrives at the following representation of the Hamiltonian:

$$\begin{aligned} \mathcal{H}' = & \sum_{\mu=c,s,f,sf} \sum_k \epsilon_k \psi_{\mu,k}^\dagger \psi_{\mu,k} - eV_c(t) \hat{N}_c + eV(t) \hat{N}_f \\ & + i\mu_B g_i \hat{H} \hat{b} \hat{a} + i \frac{J^+}{2\sqrt{\pi a L}} \sum_k (\psi_{sf,k}^\dagger + \psi_{sf,k}) \hat{b} \\ & + \frac{J_\perp^{LR}}{2\sqrt{\pi a L}} \sum_k (\psi_{f,k}^\dagger - \psi_{f,k}) \hat{a} \\ & + \frac{J^-}{2\sqrt{\pi a L}} \sum_k (\psi_{sf,k}^\dagger - \psi_{sf,k}) \hat{a}. \end{aligned} \quad (3)$$

Here J^\pm are equal to $(J_\perp^{LL} \pm J_\perp^{RR})/2$; the energies ϵ_k are equal to $\hbar v_F k$; \hat{N}_c and \hat{N}_f are the number operators for the charge and flavor fermions, respectively; $V_c(t)$ and $V(t)$ are equal to $V_L(t) + V_R(t)$ and $V_R(t) - V_L(t)$, respectively; a is an ultraviolet momentum cutoff, corresponding to a lattice spacing; and L is the effective size of the system (i.e., k is discretized according to $k = 2\pi n/L$). Within this mapping, the Hamiltonian term \mathcal{H}_0 is reduced to the free kinetic-energy part of Eq. (3), \mathcal{H}'_{kin} ,

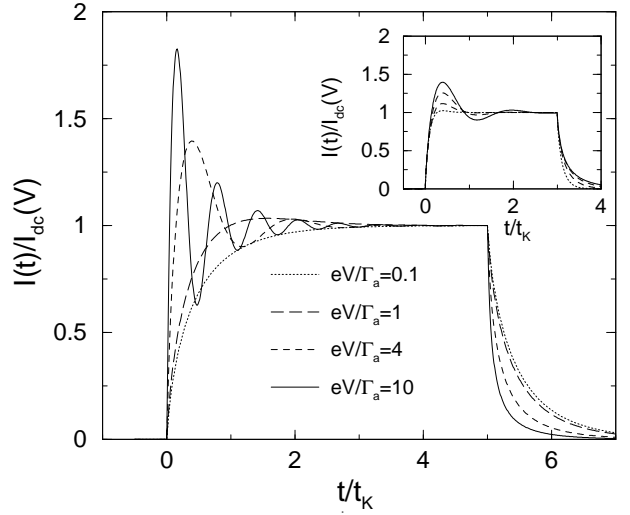


FIG. 1. The time-dependent current $I(t)$ in response to an eV bias potential that is switched on at time $t = 0$, and then switched off again at time $t = \tau$. Here $\tau = 5t_K$ with $t_K = \hbar/\Gamma_a$, $k_B T$ is fixed at $0.1\Gamma_a$, and $I_{dc}(V)$ is the steady-state current for a dc voltage bias of eV [see Eq. (7)]. As eV is increased, oscillations develop in $I(t)$, leading to a significant reduction in the rise time. The saturation time, however, is unaffected by the bias at the solvable point. Inset: Temperature dependence of $I(t)$ for fixed $eV/\Gamma_a = 4$ and $\tau/t_K = 3$. Full, long-dashed, dashed, and dotted lines correspond to $k_B T/\Gamma_a = 0.1, 0.5, 1$ and 2 , respectively. With increasing T , the saturation time is reduced and the current oscillations are suppressed.

and so ρ_0 is transformed to $e^{-\beta\mathcal{H}'_{kin}}/\text{Trace}\{e^{-\beta\mathcal{H}'_{kin}}\}$.

Having converted the problem to a noninteracting form, one can sum exactly all orders in the perturbation theory to obtain the current. The solution features two basic energy scales,^{9,11} $\Gamma_a = [(J_\perp^{LR})^2 + (J^-)^2]/4\pi a\hbar v_F$ and $\Gamma_b = (J^+)^2/4\pi a\hbar v_F$, which determine the width of the different Majorana spectral functions, and thus play the role of Kondo temperatures.¹⁶ The conventional one-channel Kondo effect is best described by the case where $\Gamma_a = \Gamma_b$, for which only a single Kondo scale emerges.⁹

Following Plihal *et al.*,¹³ we begin with the case of a pulsed bias potential and a zero magnetic field. Explicitly, we assume that a bias potential of eV is switched on at time $t = 0$, and then switched off again at time $t = \tau$. Denoting $(J_\perp^{LR})^2/4\pi a\hbar v_F$ by Γ_1 , the resulting time-dependent current $I(t)$ flowing from right to left is conveniently expressed via the auxiliary function

$$\mathcal{J}(t; V_1, V_2) = \frac{e\Gamma_1}{\pi\hbar} \sum_{n=0}^{\infty} e^{-[(2n+1)\pi k_B T + \Gamma_a]t/\hbar} \times \left(\frac{1}{n + \frac{1}{2} + \frac{\Gamma_a + ieV_1}{2\pi k_B T}} - \frac{1}{n + \frac{1}{2} + \frac{\Gamma_a + ieV_2}{2\pi k_B T}} \right). \quad (4)$$

For $t \leq 0$, $I(t)$ is obviously zero. For $0 \leq t \leq \tau$ it equals

$$I_1(t) = I_{dc}(V) - \text{Im} \left\{ e^{-ieVt/\hbar} \mathcal{J}(t; 0, V) \right\}, \quad (5)$$

while for $\tau \leq t$ it is given by

$$I_2(t) = \text{Im} \{ \mathcal{J}(t-\tau; 0, V) \} - \text{Im} \left\{ e^{-ieV\tau/\hbar} \mathcal{J}(t; 0, V) \right\}. \quad (6)$$

Here $I_{dc}(V)$ is the steady-state current for an eV dc voltage bias:⁹

$$I_{dc}(V) = \frac{e\Gamma_1}{\pi\hbar} \text{Im} \left\{ \psi \left(\frac{1}{2} + \frac{\Gamma_a + ieV}{2\pi k_B T} \right) \right\}. \quad (7)$$

The relevant time scales for the evolution of the current are easily read off from Eqs. (5) and (6). As proposed by Plihal *et al.*,¹³ for $0 \leq t \leq \tau$ the current has two components: a constant term equal to the new steady-state current, and a transient term that oscillates with frequency $\omega = eV/\hbar$. The latter component involves two natural times scales: the period of oscillations $t_v = 2\pi\hbar/eV$, and the basic decay time $t_d = \hbar/(\Gamma_a + \pi k_B T)$, which enters via $\mathcal{J}(t, 0, V)$. For $t_d \ll t_v$, the current saturates before any oscillations develop. Hence the rise and saturation times are both of the order of t_d . On the other hand, for $t_v < t_d$ the current oscillates before saturating at $I_{dc}(V)$, resulting in a much shorter rise time. Specifically, the rise time is identified with the first instance at which the transient term vanishes. Writing $\mathcal{J}(t; 0, V)$ of Eq. (4) as $|\mathcal{J}(t; 0, V)|e^{i\varphi(t)}$, it is simple to show that $0 < \varphi(t) < \frac{\pi}{2}$. As the transient current vanishes each time $eVt/\hbar - \varphi(t)$ equals an integer multiple of π , this first happens at some time shorter than $t_v/4$. Thus, while the saturation time still follows t_d , the rise time is bounded by $t_v/4 \ll t_d$. This transition in rise time from approximately t_d to less than $t_v/4 \ll t_d$ is clearly seen in Fig. 1, where the time-dependent current is plotted for increasing values of eV .

Contrary to the current oscillations that may develop for $0 \leq t \leq \tau$, the fall off for $t > \tau$ is described in Eq. (6) by the difference of two non-oscillatory terms, each of which decays to zero. While the tail of the fall off is always characterized by the fall-off time t_d , the initial stages of the drop do not typically follow a single time scale. This is best seen for long pulse durations, $\tau \gg t_d$, when only the first term survives in Eq. (6). To this end, consider $\text{Im}\{\mathcal{J}(t-\tau; 0, V)\}$ with $t = \tau$ and $t_v < t_d$. Using the series representation of Eq. (4), an increasing number of terms contribute to $\text{Im}\{\mathcal{J}(0; 0, V)\}$ as eV is increased, typically up to $n \sim eV/2\pi k_B T$. For $t > \tau$, each of these terms decays with a separate relaxation time, $t_d^{(n)} = \hbar/[(2n+1)\pi k_B T + \Gamma_a]$, such that the total signal contains a range of time scales from $\sim t_v$ up to t_d . While all time scales participate in the early stages of the fall off, the tail is governed by the longest time scale, t_d .

For shorter pulse durations, $\tau \sim t_v < t_d$, the fall-off current is actually quite sensitive to the precise value of τ . This is demonstrated in Fig. 2, where several pulse durations are plotted for fixed $eV/\Gamma_a = 10$. Although $eV/\Gamma_a = 10$ may appear too large a bias for the application of the solvable point, the qualitative agreement with

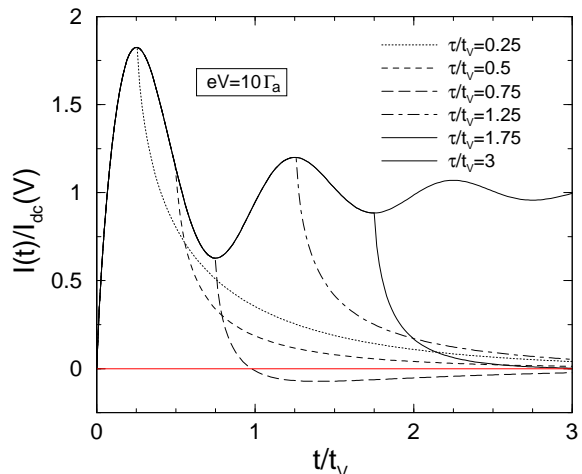


FIG. 2. The current $I(t)$ in response to a pulsed bias potential of magnitude $eV = 10\Gamma_a$, for different pulse durations τ . Here $k_B T = 0.1\Gamma_a$ and $t_v = 2\pi\hbar/eV$. $I_{dc}(V)$ is the steady-state current for an eV dc voltage bias. The asymptotic fall-off current oscillates with $\sin(2\pi\tau/t_v)$, resulting in the reversal of the current for $\tau/t_v = 3/4$.

the numerical calculations of Plihal *et al.* (see Ref. 13, Fig. 3) is strikingly good. In fact, we are even able to reproduce the reversal of the fall-off current for certain pulse lengths. To understand the origin of this somewhat surprising effect, we go back to Eq. (6) with a sufficiently large $t - \tau$, such that each \mathcal{J} function can be roughly approximated by the $n = 0$ term in Eq. (4) (we assume $T > 0$). For a large voltage bias such that $eV \gg \Gamma_a$ and $eV \gg \pi k_B T$ (as is the case in Fig. 2), the fall-off current of Eq. (6) is asymptotically given by

$$I_2(t) \sim \frac{2k_B T \Gamma_1}{\hbar V} e^{-(t-\tau)/t_d} \left[1 - e^{-\tau/t_d} \cos \left(2\pi \frac{\tau}{t_v} \right) + \frac{2\pi t_d}{t_v} e^{-\tau/t_d} \sin \left(2\pi \frac{\tau}{t_v} \right) \right]. \quad (8)$$

Thus, since $t_d \gg t_v$ and $\tau \sim t_v$ under the assumptions above, the asymptotic fall-off current is dominated by the last term in Eq. (8). Consequently, the sign of $I_2(t)$ oscillates with $\sin(2\pi\tau/t_v)$, precisely as seen in Fig. 2.

Although our solution clearly captures the essential findings of the non-crossing approximation, there are two major omissions to be noted. First, working with a Kondo impurity rather than an Anderson impurity, our model lacks the short charge-fluctuation time scale ($t_0 = \hbar/\Gamma_{\text{dot}}$ in the notations of Ref. 13), which governs the very early response of a quantum dot to the abrupt change in the applied voltage bias. Second, for $0 < t \leq \tau$, our solution does not show the expected decrease in saturation time for large voltage bias.¹³ This decrease, which stems from the dissipative lifetime induced by the bias potential,¹⁴ is not captured by the solvable point. On the other hand, our solution gives a very transparent picture for the role of a temperature. As the temperature is increased, t_d crosses over from \hbar/Γ_a to $\hbar/\pi k_B T$, which re-

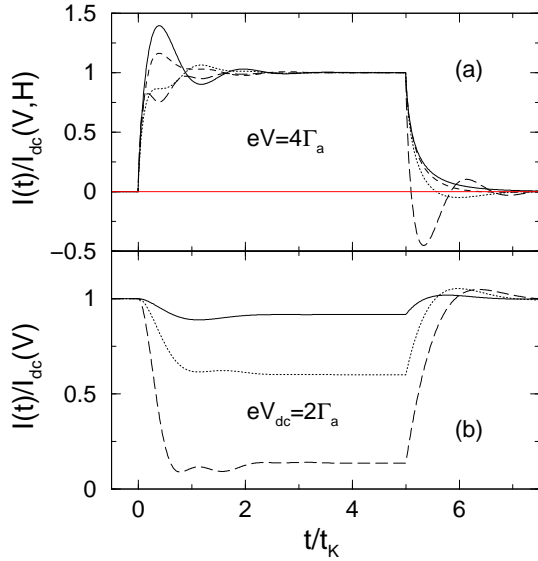


FIG. 3. The time-dependent current for (a) a dc magnetic field H and a rectangular pulsed bias potential of magnitude $eV = 4\Gamma_a$; and (b) a dc bias potential $eV = 2\Gamma_a$ and a rectangular pulsed magnetic field of magnitude H . Upper panel: Solid, dashed, dotted, and long-dashed lines correspond to $\mu_B g_i H / \Gamma_a = 0, 1, 2,$ and $4,$ respectively. Lower panel: Solid, dotted, and long-dashed lines correspond to $\mu_B g_i H / \Gamma_a = 1, 2,$ and $4,$ respectively. In both cases, the pulse duration is $\tau = 5t_k$ ($t_k = \hbar / \Gamma_a$), and the temperature is equal to $k_B T / \Gamma_a = 0.1$. $I_{dc}(V, H)$ marks the steady-state current for a dc voltage bias of eV and a dc magnetic field H .

mains the only relevant time scale for $k_B T \gg eV$. Thus, all response times for the current are determined by the temperature in this limit.

An important advantage of the solvable point with $\Gamma_a = \Gamma_b$ is the ability to incorporate an arbitrary time-dependent magnetic field. Specifically, we find that the current $I(t)$ for a general voltage bias $eV(t)$ and an arbitrary field $H(t)$ is equal to $\frac{1}{2} [I_+(t) + I_-(t)]$, where $I_{\pm}(t)$ is the current for a zero magnetic field and an effective bias potential $eV_{\pm}(t) = eV(t) \pm \mu_B g_j H(t)$. The latter bias has a simple physical interpretation. When an electron tunnels by flipping the impurity spin, the effective potential barrier it sees is equal to $eV_{\pm}(t)$, depending on the initial impurity state, and the direction of tunneling.

Using the above decomposition of $I(t)$ into $I_{\pm}(t)$, we have computed the current for the two opposite cases of (i) a dc magnetic field H and a rectangular pulsed bias potential of magnitude eV , and (ii) a dc bias potential of eV and a rectangular pulsed magnetic field of magnitude H . In both cases, the pulse duration was taken to be τ , with the corresponding field being equal to zero for $t < 0$ and $t > \tau$. The calculation of $I_{\pm}(t)$ in each of these cases requires the generalization of Eqs. (5)–(6) to a pulsed bias potential of the form $V(t) = V_2$ for $0 \leq t \leq \tau$ and $V(t) = V_1 \neq 0$ otherwise, which gives

$$I_1(t) = I_{dc}(V_2) - \text{Im} \left\{ e^{-ieV_2 t / \hbar} \mathcal{J}(t; V_1, V_2) \right\}, \quad (9)$$

$$I_2(t) = I_{dc}(V_1) + \text{Im} \left\{ e^{-ieV_1(t-\tau)/\hbar} \mathcal{J}(t-\tau; V_1, V_2) \right\} - \text{Im} \left\{ e^{-ieV_2 \tau / \hbar} e^{-ieV_1(t-\tau)/\hbar} \mathcal{J}(t; V_1, V_2) \right\}. \quad (10)$$

For $t \leq 0$, the corresponding current is obviously $I_{dc}(V_1)$.

The resulting $I(t)$ curves are depicted in Fig. 3. As is clearly seen, the combination of a bias and a magnetic field produces nontrivial interference patterns with several underlying time scales. These include t_d , $t_{\pm} = 2\pi\hbar / |eV \pm \mu_B g_i H|$, and either $t_h = 2\pi\hbar / \mu_B g_i H$ or t_v , depending on whether one is dealing with a pulsed bias potential or a pulsed magnetic field. In particular, for a pulsed bias potential and moderately large dc magnetic fields, there are current oscillations in the fall-off current, with a characteristic frequency of $\omega = \mu_B g_i H / \hbar$. Such effects should be observable in ultra small quantum dots.

- ¹ D. Goldhaber-Gordon *et al.*, Nature **391**, 156 (1998); D. Goldhaber-Gordon *et al.*, Phys. Rev. Lett. **81**, 5225 (1998).
- ² S. M. Cronenwett *et al.*, Science **281**, 540 (1998).
- ³ J. Schmid *et al.*, Physica B **258**, 182 (1998).
- ⁴ F. Simmel *et al.*, Phys. Rev. Lett. **83**, 804 (1999).
- ⁵ P. W. Anderson, Phys. Rev. **124**, 41 (1961).
- ⁶ U. Gerland *et al.*, Phys. Rev. Lett. **84**, 3710 (2000).
- ⁷ J. Appelbaum, Phys. Rev. Lett. **17**, 91 (1966); P. W. Anderson, Phys. Rev. Lett. **17**, 95 (1966).
- ⁸ L. I. Glazman and M. E. Raikh, Pis'ma Zh. Eksp. Teor. Fiz. **47**, 378 (1988) [JETP Lett. **47**, 453 (1988)]; T. K. Ng and P. A. Lee, Phys. Rev. Lett. **61**, 1768 (1988); S. Hershfield, J. H. Davies, and J. W. Wilkins, Phys. Rev. Lett. **67**, 3720 (1991); Y. Meir, N. S. Wingreen, and P. A. Lee, Phys. Rev. Lett. **70**, 2601 (1993).
- ⁹ A. Schiller and S. Hershfield, Phys. Rev. B **51**, 12896 (1995); A. Schiller and S. Hershfield, *ibid.* **58**, 14978 (1998).
- ¹⁰ M. H. Hettler and H. Schoeller, Phys. Rev. Lett. **74**, 4907 (1995); T. K. Ng, Phys. Rev. Lett. **76**, 487 (1996); Y. Goldin and Y. Avishai, Phys. Rev. Lett. **81**, 5394 (1998); A. Kaminski *et al.*, Phys. Rev. Lett. **83**, 384 (1999).
- ¹¹ A. Schiller and S. Hershfield, Phys. Rev. Lett. **77**, 1821 (1996).
- ¹² For a first application of ac fields to a quantum dot in the Kondo regime, see J. M. Elzerman *et al.*, J. Low Temp. Phys. **118**, 375 (2000).
- ¹³ M. Plihal, D. C. Langreth, and P. Nordlander, Phys. Rev. B **61**, 13341 (2000).
- ¹⁴ N. S. Wingreen and Y. Meir, Phys. Rev. B **49**, 11040 (1994).
- ¹⁵ G. Toulouse, Phys. Rev. B **2**, 270 (1970).
- ¹⁶ V. J. Emery and S. Kivelson, Phys. Rev. B **46**, 10812 (1992).
- ¹⁷ The Toulouse limit was also applied to a different type of nonequilibrium dynamics, i.e., that of a dissipative multiwell system. See U. Weiss and M. Wollensak, Phys. Rev. B **37**, 2729 (1988); U. Weiss *et al.*, Z. Phys. B **84**, 471 (1991).